

1  
2  
3  
4  
5  
6  
7  
8  
9  
10  
11  
12  
13  
14  
15  
16  
17  
18  
19  
20  
21  
22  
23  
24  
25  
26  
27  
28  
29  
30  
31  
32  
33  
34  
35

# Technical Note:

## **Spectral slopes in deep, weakly-stratified ocean and coupling between sub-mesoscale motions and small-scale mechanisms**

**by Hans van Haren**

Royal Netherlands Institute for Sea Research (NIOZ), P.O. Box 59, 1790 AB Den Burg,  
the Netherlands.

e-mail: [hans.van.haren@nioz.nl](mailto:hans.van.haren@nioz.nl)

36 Short summary. Large ocean circulations include small-scale physical processes like transport  
37 by sub-mesoscale eddies and turbulence by internal wave breaking. Knowledge is lacking on  
38 precise interaction between different processes. In deep weakly stratified waters, continuous  
39 spectral slopes are observed that extend from sub-mesoscales across the internal wave band to  
40 turbulence range. Such cross-spectral correspondence is suggested a potential feedback  
41 mechanism stabilizing large-scale ocean circulations.

42

43 **Abstract.** Large, basin-wide ocean circulations are complex nonlinear dynamical systems.  
44 They include small-scale physical processes such as, for example, transport by sub-mesoscale  
45 eddies and turbulence-generating breaking of internal waves. To date however, knowledge is  
46 lacking on precise interaction between different processes. In this note, a potential contributor  
47 to interaction is investigated using spectra from deep-sea moored observations. In weakly  
48 stratified waters, continuous spectral slopes are observed that extend from sub-mesoscales  
49 across the internal wave band to turbulence range. In the latter, the governing slope can be  
50 distinctly different from the inertial subrange of shear turbulence and is described as the  
51 buoyancy subrange of convection turbulence. At sub-inertial frequencies, the slope's  
52 extension either describes quasi-gyrosopic waves or sub-mesoscale eddies. Such cross-  
53 spectral correspondence is suggested a potential feedback mechanism stabilizing large-scale  
54 ocean circulations.

55

## 56 **1 Introduction**

57 The extent of anthropogenic influence on the Earth's climate warrants studies of the  
58 ocean as a major player. Large, basin-wide ocean circulations are important for transporting  
59 properties like heat, carbon and nutrients. Schematically, the Atlantic(-Ocean) Meridional  
60 Overturning Circulation (AMOC) is depicted to transport heat from the equator to the poles  
61 near the surface and carbon in the abyssal return (e.g., Aldama-Campino et al., 2023). It  
62 includes physical processes like 'deep dense-water formation' in the polar region. Recent  
63 mathematical and numerical modelling such as based on varying single parameters like sea-

64 surface temperature (e.g., Ditlevsen and Ditlevsen, 2023) and freshwater influx (e.g., van  
65 Westen et al., 2024) suggest a potential future collapse of the AMOC. It is argued that this  
66 may have consequences for Northwest-European climate.

67         Whilst the modelling might be robust mathematically, it lacks physical processes of  
68 the drivers of the AMOC and observational evidence thereof. This will have consequences for  
69 the feedback mechanisms at work in the nonlinear dynamical system of ocean circulation. As  
70 has been reviewed for AMOC numerical models (Gent, 2018), important feedback  
71 mechanisms are vertical turbulent mixing, sub-mesoscale gyre ‘eddy’ transport, and the  
72 coupling with the atmosphere. Here we elaborate on the importance of turbulence induced by  
73 internal wave breaking, possibly coupling with sub-mesoscale eddies (e.g., Chunchuzov et al.,  
74 2021), and stability variations in vertical density stratification for such feedback, by  
75 reviewing insights from recent modeling and deep-sea observations. In particular as an  
76 example for complexity of dynamical system interactions, the core of ocean motions is  
77 spectrally investigated focusing on most energetic mesoscale, internal wave, and turbulence  
78 scales, for deep weakly stratified waters.

79         In contrast with the atmosphere, the ocean is not an effective heat engine (Wunsch  
80 and Ferrari, 2004) despite its heat transportation. As a result, the AMOC is not predominantly  
81 buoyancy-driven via push by deep dense-water formation near the poles (Marshall and Schott,  
82 1999; Marotzke and Scott, 1999), which notably occurs in sporadic pulses rather than  
83 continuously. Instead, the AMOC is mainly wind-steered (e.g., Liu et al., 2024) and tide-  
84 driven, with turbulent mixing by internal wave breaking, and possibly associated upwelling  
85 close to boundaries (Ferrari et al., 2016; McDougall and Ferrari, 2017), being considered an  
86 important physics process of pull that dominates over push by a heat engine. Winds, near the  
87 ocean surface, and tides, via interaction with seafloor topography deeper down, contribute  
88 about equally to generate internal waves that are found everywhere in the ocean interior. Such  
89 waves break predominantly at ubiquitous underwater seamounts and continental slopes.

90         Without turbulent mixing, the AMOC would be confined to a 100-m thick near-  
91 surface layer and the deep-ocean would be a stagnant pool of cold water (Munk and Wunsch,

1998). This is not the case however, and the solar heat is mixed from the surface downward so that the ocean is stably stratified in density all the way into its deepest trenches, as has been shown in hydrographic deep-ocean observations (Taira et al., 2005; van Haren et al., 2021a). Although turbulent mixing by internal wave breaking in the ocean-interior is insufficient by at least a factor of two to maintain the vertical density stratification (e.g., Gregg, 1989, Polzin et al., 1997), such breaking along ocean boundaries has been suggested to be more than sufficient (Munk, 1966; Polzin et al., 1997). Especially large internal wave breaking is expected to occur above steeply sloping topography (Eriksen, 1982; Thorpe, 1987; Sarkar and Scotti, 2017). Because there are more and larger seamounts than mountains on land, equally abundant sloping seafloors lead to abundant turbulent mixing, as has been charted from recent observations and modelling results summarized below.

As recent observations (van Haren and Dijkstra, 2021; van Haren et al., 2024) demonstrate that breaking waves can lead to considerable buoyancy driven convection turbulence, this note attempts further understanding of a little studied deep-sea complex process and its potential interaction with sub-mesoscale motions. The sub-inertial range of sub-mesoscale motions has rarely been a subject of oceanographic spectral observations. Knowledge about such small-scale processes and their interactions may be vital for understanding potential feedback mechanisms affecting the stability of large-scale ocean circulations.

111

## 112 **2 Recent internal wave breaking results**

Detailed observations and numerical modeling have revealed the extent of internal tide breaking processes above ocean topography (van Haren and Gostiaux, 2012; Winters, 2015; Wynne-Cattanach et al., 2024). Using high-resolution observations (e.g., van Haren and Gostiaux, 2012), internal tide breaking above steep deep-sea slopes is observed to generate spring-neap-average turbulent vertical diffusivity value of about  $3 \times 10^{-3} \text{ m}^2 \text{ s}^{-1}$ . This value is twice the value theoretically required to yield upwelling in a thin layer above sloping topography (McDougall and Ferrari, 2017). Such quantification of turbulent mixing shows

120 that it occurs with typical tidal-period-average values that are more than 100 times larger over  
121 super-critical slopes than open-ocean values. A super-critical seafloor slope is steeper than the  
122 slope of internal wave characteristics. While ocean-wide tides energetically dominate internal  
123 waves, not all seafloor slopes are super-critical for these waves. In contrast, nearly all seafloor  
124 slopes are super-critical for at least one component of secondary energetic near-inertial  
125 waves, which are generated via geostrophic adjustment following the passage or collapse of a  
126 disturbance such as fronts or atmospheric storms on the rotating Earth. Under common  
127 stratification, near-inertial waves are at the lowest frequency of freely propagating internal  
128 waves. The highest frequency propagating internal waves, near the buoyancy frequency,  
129 experience nearly vertical walls as super-critical seafloor slopes.

130         Within a tidal, or near-inertial, period, turbulence peaks in bursts of shorter duration  
131 than half an hour when highly nonlinear internal waves propagate as internal bores up a  
132 super-critical slope, once or twice a tidal cycle. The breaking of bores leads primarily to  
133 convection, buoyancy-driven turbulence, rather than frictional shear-turbulence over the  
134 sloping seafloor and occur at a wide variety of deep-sea and deep-ocean locations (e.g., van  
135 Haren et al., 2013; van Haren et al., 2024). Between bores, the turbulent mixing varies by an  
136 order of magnitude in intensity, with effects extending about 100 m vertically and several  
137 kilometers horizontally from the seafloor. Although intermittently occurring at a given  
138 position of the sloping seafloor and about 10% varying in arrival time, the turbulence is  
139 generated internally by the tide, for about 60% (Wunsch and Ferrari, 2004), and by winds, for  
140 about 40%, in a stratified ocean-environment. The turbulent bores also resuspend sediment  
141 and thereby replenish nutrients away from the seafloor (Hosegood et al., 2004), important for  
142 deep-sea life. Enhanced turbulent mixing above sloping boundaries has a demonstrated effect  
143 on the outcome of general ocean circulation models (e.g., Scott and Marotzke, 2002), with  
144 predicted subtle effects on upwelling near the seafloor (Ferrari et al., 2016).

145         The complexity of turbulence generation, mixing and restratification, are still subjects  
146 of deep-ocean research. While shear-induced turbulence has been relatively well studied in  
147 the stratified ocean, deviations such as convection-turbulence are little observed, with recent

148 exceptions (van Haren and Dijkstra, 2021; van Haren et al., 2024). Convection turbulence is  
149 dominant in the atmosphere especially during daytime, and has also been observed in the  
150 near-surface ocean during nighttime (e.g., Brainerd and Gregg, 1995), but it has never been  
151 quantitatively directly observed in deep dense-water formation zones (Thorpe, 2005) and  
152 above geothermal vents. Lagrangian float measurements yielded average vertical heat flux  
153 estimates due to convection reaching down to 1000 m from the surface in the Labrador Sea  
154 (Steffen and D'Asaro, 2002). It would be challenging to set-up an experiment in which such  
155 floats are equipped with microstructure instrumentation, and be able to measure convection  
156 turbulence from the surface down to the deep seafloor.

157         Deep dense-water formation does not only occur in polar seas, but occasionally also  
158 in the at least 10°C warmer Mediterranean (Gascard, 1978), with an important contribution of  
159 atmospheric exchange due to orographic generated winds affecting the preconditioning by  
160 cooling and drying of near-surface waters. Similarly, internal waves occur in oceans and in  
161 the Mediterranean under stratification conditions that vary over at least one order of  
162 magnitude in time and space, but tides are relatively weak in the Mediterranean, and yet  
163 'sufficient' turbulent diapycnal mixing, sufficient for maintenance of deep-sea stratification  
164 and thereby driving overturning circulation, is generated via the breaking above topography  
165 of near-inertial motions mainly (van Haren et al., 2013). Further complications are expected  
166 from interactions of internal waves with sub-mesoscale eddies and potential consequences of  
167 varying intensity thereof, e.g., on seasonal scales.

168

### 169 **3 Mediterranean observations as an example proxy for ocean conditions**

170         In many physical oceanographic aspects of heat and salt budgets, large-scale water-  
171 flow circulation, strong boundary flow, eddies at sub-mesoscales, near-inertial motions  
172 including gyroscopic waves and internal wave turbulence, the Mediterranean Sea can be  
173 considered a sample for the state of the much larger oceans (e.g., Gascard, 1973; Crepon et  
174 al., 1982; Garrett, 1994; Millot, 1999; van Haren and Millot, 2004; Testor and Gascard,

175 2006). Like in oceans, the Mediterranean seafloor reaches great depths and can be rugged  
176 with steep slopes in places, including continental slopes incised by deep canyons.

177         In the Northwest Mediterranean, vertical density stratification varies markedly with  
178 seasons and years, having relatively large near-surface values in summer and relatively low  
179 values in winter. The proximity of extensive mountain ranges on land generates highly  
180 variable winds that can cool and dry surface waters. In winter in weaker stratified waters, this  
181 may lead to unstable conditions of buoyancy driven convection in an exchange of dense-water  
182 sinking down, and less dense-waters up. Like in the polar regions, such exchange can be  
183 observed daily in the upper 10 m from the sea-surface, regularly down to a few 100 m from  
184 the surface, and seldom, once every 5-8 years (e.g., Rhein, 1995; Mertens and Schott, 1998),  
185 down to the abyssal seafloor at about 2500 m. In contrast, horizontal density gradients  
186 associate with forcing of a dynamically unstable boundary current and eddies at multiple 1-  
187 100 km sub-mesoscales (e.g., Crepon et al., 1982; Testor and Gascard, 2006). These eddy  
188 motions may push relatively warm waters down, thereby increasing the weak stratification in  
189 the deep-sea.

190         In summer, atmospheric disturbances are less intense, near-surface stratification is  
191 large due to solar heating, and eddy activity associated with some continental boundary flows  
192 is weaker (Albérola et al., 1995). This opens the possibility for detection of near-inertial wave  
193 dominance in kinetic energy. In relatively strong stratification, mainly gravity-driven parts of  
194 near-inertial waves generate largest vertical current differences ‘shear’ that destabilize  
195 stratification due to their relatively short vertical length-scale, not only in the Mediterranean  
196 but also as observed in the Atlantic Ocean (van Haren, 2007). This destabilization may lead to  
197 small-10-m vertical scale layering of near-homogeneous waters throughout seas and oceans.  
198 On larger-100-m vertical scales near-homogeneous waters occur in deep waters of the  
199 Mediterranean as well as of North-Atlantic basins like the Bay of Biscay and Canary Basin.  
200 In near-homogeneous water-layers with weak stratification, gyroscopic, Earth-rotation-driven,  
201 parts of near-inertial waves dominate and result in 0.1-1 km diameter smaller than sub-  
202 mesocale tubes of slantwise rather than vertical convection (Emanuel, 1994; Marshall and

203 Schott, 1999; van Haren and Millot, 2004). Hence, one may expect frequency spectra of non-  
204 tidal dominated data from instruments moored in the Mediterranean reveal convection and  
205 thus deep transport under winter and summer conditions.

206 It is noted that ocean-spectra, such as frequency spectra of kinetic energy and scalar  
207 quantities like temperature from data registered by moored instrumentation, may show peaks  
208 such as at narrowband tidal and at, broader band, inertial frequencies, but they lack gaps. This  
209 lack of spectral gaps potentially couples motions at sub-inertial with inertial-buoyancy  
210 internal wave with super-buoyancy turbulence frequency ranges. However, it is unclear how  
211 such a coupling may work as some motions represent two-dimensional ‘2D’ eddies, some  
212 linear waves, some non-linear waves, some anisotropic, quasi 3D, stratified turbulence, and  
213 some isotropic 3D turbulence. This is investigated by renewed spectral analysis below, using,  
214 in analogy, slopes typical for investigating energy cascades in turbulence research.

215

#### 216 **4 Uncommon slopes in revisited spectra**

217 Kinetic energy (KE) spectra from historic moored current meter observations down to  
218 mid-depth  $z = -1100$  m in the Ligurian Sea under upper-sea strongly stratified ‘summer’ and  
219 weakly stratified ‘winter’ conditions surely lack gaps (Fig. 1). Year-round at  $z = -1100$  m, the  
220 buoyancy frequency  $N$ , reflecting the square-root of vertical density stratification, is small  $N$   
221  $\sim O(f)$ ,  $f$  denoting the inertial frequency involving Earth rotation. This narrows the local  
222 internal wave band, while, especially in winter, sub-mesoscale activity is large in the area,  
223 and, occasionally, the few moored current meter temperature records showed inversions (van  
224 Haren and Millot, 2003). Although these hourly sampled data barely resolve the turbulence  
225 ranges at frequencies  $\omega > N$ , the internal wave continuum was suggested to scale like  $\omega^p$ ,  
226 with, on a log-log plot, ‘spectral slope’  $p = -2.2 \pm 0.4$ , independent of location and season  
227 albeit with different KE (power) levels.

228 Within the uncertainty range, several possible explanations can be given for the  
229 observed spectral slope. Freely propagating internal gravity waves have been fitted to  $p = -$



230  $2 \pm 0.5$  but only for  $f \ll \omega \ll N$  (Garrett and Munk, 1972). Considering that the data in Fig. 1  
231 are from a site where locally  $N = (3 \pm 2)f$ , irrespective of season (van Haren and Millot, 2003),  
232 alternative explanations were sought for observed spectral slopes at sub-inertial frequencies  
233  $0.2 \text{ cpd} < \omega < f$ . Cpd is short for ‘cycles per day’. An obvious candidate is ‘fine-structure  
234 contamination’ of step functions passing sensors, which gives a theoretical value of  $p = -2$   
235 (Phillips, 1971; Reid, 1971). For their winter data, van Haren and Millot (2003) attributed  
236 such a slope to evidence intense mesoscale activity, because of the continuation of slope up to  
237  $\omega = 5 \text{ cpd}$  before rolling off near the Nyquist frequency. However, they did not elaborate.  
238 Below, the data in Fig. 1 are re-analyzed from the perspective of convection-turbulence.

239         Theoretical considerations of non-zero-mean flow convection-turbulence suggest a  
240 spectral scaling in the buoyancy subrange having  $p = -11/5 = -2.2$  for KE, and  $p = -7/5$  for an  
241 active scalar quantity. This ‘BO’-scaling follows atmospheric and theoretical works by  
242 Bolgiano (1959) and Obukhov (1959). The scaling was set-up for a stably stratified  
243 atmospheric environment for the anisotropic part in which turbulent kinetic energy is partially  
244 transferred to potential energy leading to turbulent convection. Later works extended BO-  
245 scaling to purely buoyancy-driven turbulence, e.g., for Rayleigh-Bénard convection (Lohse  
246 and Xia, 2010) and Rayleigh-Taylor instabilities (Poujade, 2006; Celani et al., 2006).

247         Laboratory experiments on such gravitationally driven convection are inconclusive on  
248 BO-scaling. On the one hand, this scaling is confirmed for both KE and temperature in  
249 experiments by Ashkenazi and Steinberg (1999), while on the other hand it is only confirmed  
250 for scalars by Pawar and Arakeri (2016) who found a slope of  $p = -5/3$  for KE. The  $p = -5/3$ -  
251 slope suggests dominance of shear-induced turbulence of the inertial subrange for equilibrium  
252 isotropic turbulence cascade in the ‘KO’-scaling (Kolmogorov, 1941; Obukhov, 1949) but  
253 should also be found in spectra of scalars that are passive in this range. While Liot et al.  
254 (2016) show KO-scaling in their model that may have to do with their Lagrangian data as  
255 proper transfer brings the data closer to BO-scaling, Poujade (2006) and Cenari et al. (2006)  
256 show clear BO-scaling in their models. This suggests particular conditions do affect the

257 dominance of shear- or convection-turbulence. It is noted that BO-scaling is also simply  
 258 considered as a significant deviation from KO-scaling, which is more commonly observed in  
 259 stratified shear flows.

260 Obviously, scalars cannot be passive and active at the same time and in the same  
 261 space. This discrepancy between types of scaling between scalars and KE may be because the  
 262 laboratory experiments of Pawar and Arakeri (2016) were in zero mean flow. Also, under  
 263 sufficiently stable conditions without shear, no inertial subrange is expected (Bolgiano, 1959).  
 264 However, the spectral extent of BO-scaling is largely unknown albeit it is more generally  
 265 found adjacent to higher-frequency inertial subrange. While KO-scaling is based on a forward  
 266 cascade of energy, the direction of energy cascade is inconclusive for BO-scaling and may be  
 267 partially forward and partially backward, at least as reasoned for pure buoyancy-driven  
 268 convection-turbulence (Lohse and Xia, 2010). Probably, directions of cascade change with  
 269 locality in the flow, and perhaps depend on scale, which would also imply that KO- and BO-  
 270 scaling cannot be found at the same site.

271 Revisiting data from non-zero mean flow and weakly stratified deep-sea in Fig. 1  
 272 demonstrates the possibility of fit of  $p = -11/5$  outside near-inertial harmonic peaks. In winter,  
 273 such a fit is observed consistently through the entire range of  $0.2 < \omega < 5$  cpd. In traditional  
 274 terms, this frequency range covers the transition from mesoscale  $\omega < f$ , via internal wave  $f <$   
 275  $\omega < N$ , to turbulence  $\omega > N$  motions. In summer, the  $p = -11/5$ -slope is found at two different  
 276 KE levels for bands  $0.2 < \omega < \omega_{\min}$  and  $2\Omega < \omega < 5$  cpd at sub- and super-IGW frequencies,  
 277 respectively. Here,  $\omega_{\min} \leq f$  denotes the minimum frequency bound for inertio-gravity waves  
 278 IGW (LeBlond and Mysak, 1978), and  $\Omega$  the Earth rotational frequency. Maximum IGW  
 279 frequency is denoted by  $\omega_{\max} \geq 2\Omega$ ,  $N$ . The  $\omega_{\min}$  and  $\omega_{\max}$  are functions of  $N$ , latitude  $\varphi$  and  
 280 direction of wave propagation (LeBlond and Mysak, 1978; Gerkema et al., 2008),

$$281 \quad \omega_{\max}, \omega_{\min} = (A \pm (A^2 - B^2)^{1/2})^{1/2} / \sqrt{2}, \quad (1)$$

282 in which  $A = N^2 + f^2 + f_s^2$ ,  $B = 2fN$ , and  $f_s = f_h \sin \alpha$ ,  $\alpha$  the angle to  $\varphi$ . For  $f_s = 0$  or  $N \gg 2\Omega$ ,  
 283 the traditional bounds  $[f, N]$  are retrieved from (1). The plotted IGW-bounds  $[\omega_{\min}, \omega_{\max}]$  are

284 for weakly stratified, near-homogeneous layers in which  $N = f$ . This weak stratification would  
285 lead to an impossible wave solution under the traditional approximation, but (1) allows wave  
286 propagation, albeit horizontally for one component (e.g., Gerkema et al., 2008).

287         The bridge between the KE-levels at sub- and super-IGW is formed by the finitely  
288 broad near-inertial peak. The base of this peak is proposed to slope like  $p = -1$  reaching super-  
289 IGW BO-scaling at about  $\omega \approx 4 \text{ cpd} \approx N$ . Such  $p = -1$ -slope has been observed for the KE-  
290 spectral continuum between  $[f N]$  from the deep Bay of Biscay, Northeast Atlantic Ocean  
291 (van Haren et al., 2002). Theoretically, this slope represents spectral scaling of intermittency  
292 of a weakly chaotic nonlinear system (Schuster, 1984), i.e., 3D dynamical systems that evolve  
293 into self-organized critical structures of states which are minimally stable (Bak et al., 1987).  
294 Such a spectral bridge, or hump, is expected for turbulence in unstable stratification, as has  
295 been illustrated using atmospheric observations (Lin, 1969). It is attributed to the flow field  
296 absorbing energy from the scalar temperature field as potential energy is transferred to kinetic  
297 energy. It is not clear to what extent near-inertial internal waves contribute in a similar way to  
298 spectral redistribution of energy in our oceanographic data. As the observations from the  
299 central Ligurian Sea show similar results, the hump is unlikely associated with seafloor slopes  
300 matching the slope of near-inertial internal wave rays.

301         These spectral observations suggest a dominance of convection cascade from sub-  
302 meso- via IGW- to, probably because unresolved, turbulence-scales under high-energetic  
303 winter-conditions as they show a continuous slope across their frequency ranges. Such a  
304 cascade is also suggested under quieter summer conditions when, however, it is masked by  
305 IGW that lead a cascade at  $\omega > \omega_{\min}$ . Especially the sub-inertial range of apparent BO-scaling  
306 seems out of the turbulence range, unless waters are near-homogeneous  $N \rightarrow 0$  so that  $\omega_{\min} \rightarrow$   
307  $0$ , from (1). This would extend not only IGW, notably gyroscopic waves, but also turbulence,  
308 probably in the form of slantwise convection, to the sub-mesoscale range.

309         For the mesoscale range, the observations in Fig. 1 are supported by numerical  
310 modeling results that have suggested eddy-KE has a broad range of spectral slopes between  $-3$

311  $< p < -5/3$  (Storer et al., 2022), and by satellite altimetry observations that indicated, after  
312 noise-correction and transfer to KE, a best-fit of  $p = -2.28$  (Xu and Fu, 2012). No mention  
313 was made of BO-scaling, but the correspondence seems evident.

314 As the KE in Fig. 1 is at least one order of magnitude larger in winter than in  
315 summer, a near-inertial peak, if it exists, will be part of the spectral continuum during the  
316 former. The winter observations suggest a continuous spread of sub-mesoscale energy across  
317 the IGW band including inertial motions and into the turbulence range. In winter, near-surface  
318 stratification is considerably weaker than in summer, so that local atmospheric-generated  
319 near-inertial motions will be smaller. It is noted that the signals near the Nyquist frequency  
320 not only contain instrumental white noise, but also unresolved turbulence motions, which are  
321 also larger in winter than in summer.

322 Inspired by Western Mediterranean observations, Saint-Guilly (1972) proposed from  
323 theoretical work that winter-time inertial KE is spread over a broad featureless band, like  
324 quasi-gyroscopic waves that may be present between IGW-bounds (1) for  $N \sim f$  (LeBlond and  
325 Mysak, 1978; Gerkema et al., 2008). However, observations from the year-round upper-layer-  
326 stratified central Western Mediterranean demonstrate that, also in deep homogeneous  $N = 0$   
327 waters, a near-inertial peak can be observed in KE-spectra (van Haren and Millot, 2004). This  
328 may be attributed to a year-round source of atmospheric-generated inertial waves that are the  
329 only internal waves that can propagate without attenuation from well-stratified to near-  
330 homogeneous layers and vice versa (van Haren, 2023b).

331 Based on limited spectral observations, Gascard (1973) suggested the generation of  
332 12-h stability waves, close to the buoyancy frequency of very weak stratification, which may  
333 briefly force dense-water formation, thereby implicitly suggesting a link between internal  
334 waves and sub-mesoscale eddies. As such eddies have estimated relative vorticity of  $|\zeta| = f/2$   
335 in the Western Mediterranean (Testor and Gascard, 2006), this addition to the planetary  
336 vorticity ( $f$ ) automatically widens the ‘effective’ near-inertial band  $0.5f < f_{\text{eff}} < 1.5f$ , of which  
337 the bounds are close to IGW-bounds for  $N = 0.8f$ . One of the properties can be a modification  
338 of near-inertial frequency (Perkins, 1976), and trapping with downward propagation of near-

339 inertial waves in anticyclonic eddies (Kunze, 1985; Voet et al., 2024). Such frequency  
340 modification may add to local physics of inertial wave caustics due to latitudinal variation  
341 (LeBlond and Mysak, 1978), which however can only lead up to 15% change in  $f$  in the  
342 Mediterranean. Although found to be limited to the rather flat KE-spectral dip in the  
343 immediate half-order-of-magnitude sub-inertial frequency band, standing vortical modes, i.e.  
344 low-frequency non-propagating motions, of vertical length-scale  $<10$  m are suggested to be as  
345 energetic as internal waves (Polzin et al., 2003). Alternatively, it has been suggested for  
346 North-Atlantic observations that vortical modes may interact with internal waves, affecting  
347 internal-wave shear that was peaking over  $O(10)$  m vertical scales at IGW-frequencies in a  
348 band with limits determined by weak stratification as in  $N = f$  (van Haren, 2007).

349 For hypothetical  $\omega_{\min} = 0.2$  cpd, at which the observed spectral slope changes away  
350 from  $p = -11/5$  (Fig. 1), one would require  $N = 0.21f$ , which is almost unmeasurable and non-  
351 existent for any prolonged period even in the deep Northwestern Mediterranean, to the  
352 knowledge of the author. However, it may reflect  $\omega_{\min}$  computed using  $f_{\text{eff}} = 0.5f$  and  $N = f_{\text{eff}}$ ,  
353 noting that such conditions can only apply for part of the record. If so, it would reflect a direct  
354 coupling between sub-mesoscale and IGW-motions with slantwise convection (Marshall and  
355 Schott, 1999; van Haren and Millot, 2004; Gerkema et al., 2008). The  $p = -11/5$  is  
356 significantly distinguishable from  $-2$  over a frequency range of nearly two orders of  
357 magnitude, and from  $-5/3$  over a range of just over half an order of magnitude (Fig. 1). The  
358 roll-off to noise (slope 0), for  $\omega > 5$  cpd, may partially be seen as following a slope of  $p = -5/3$   
359 before 0. The roll-off around 0.1 cpd suggests an unresolved broad mesoscale peak-value  
360 between 0.01 and 0.1 cpd. While these 1980's moored current meter data barely resolved the  
361 turbulence part of the KE-spectrum, and thus also not the  $p=-5/3$  inertial subrange slope, their  
362 temperature sensors were too poor to simultaneously verify any spectral scaling for scalars.

363 About 40 years later, high-resolution and high-precision moored temperature sensor  
364 'T-' data provided opportunity to verify scalar spectral scaling of turbulence energetic  
365 motions in the area. These T-data evidenced occasional warming of the deep Northwest

366 Mediterranean seafloor (Fig. 2a), which, after comparison with data from higher-up appeared  
367 to be coming from above, or slanted sideways, under relatively stratified conditions, and from  
368 general non-vents geothermal heating from below (van Haren, 2023a). The data were  
369 collected during mid-fall, when near-surface waters were well stratified and no cold, dense-  
370 water production through convection was observed. Locally near the seafloor, the broad two-  
371 day warming around day 308 is most stratified, whilst during other periods waters are only  
372 weakly stratified, including the quasi-inertial variations between days 316 and 322. These  
373 weakly stratified near-inertial, or near-buoyancy as  $N \approx f$ , temperature variations may  
374 evidence slantwise quasi-gyroscopic near-inertial waves, which can have a large vertical  
375 component (LeBlond and Mysak, 1978), as opposed to more common near-horizontal near-  
376 inertial waves in strongly stratified waters that are barely noticeable in temperature records.

377         The 18-day average spectrum of the 2-s sampled data poorly resolves sub-mesoscales  
378 but shows, near the seafloor, a well-resolved slope of  $p = -1.4 \pm 0.025$  between a large range of  
379  $0.5 < \omega < 6000$  cpd, across the IGW band and well into the turbulence band (Fig. 2b). No  
380 transition to a  $-5/3$ -slope is observed before roll-off to noise, but this does not exclude an  
381 inertial subrange at higher frequencies hidden under white noise, although shear will be  
382 limited so close to the seafloor. The observed  $p = -7/5$ -slope is found significantly different  
383 from  $p = -2$  and  $-5/3$  over the indicated frequency range of four orders of magnitude and over  
384 the range between  $100 < \omega < 10^4$  cpd thereby representing convection turbulence. Over a  
385 frequency range of half an order of magnitude the slope-error is about  $\pm 0.1$ . Albeit not greatly  
386 resolved, the range between  $\omega_{\max} < \omega < 10$  cpd falls-off more steeply roughly at  $p = -2$  and the  
387 range between  $10 < \omega < 100$  cpd shows a reduced variance that may partially be characterized  
388 by intermittency ( $p = -1$ ; Schuster, 1984), but which is not yet explained. Here, it is observed  
389 to bridge between  $p = -2$  and super-IGW BO-scaling  $p = -7/5$ . This would be further  
390 observation of a marginally ocean-state to the  $-1$ -scaling in KE-spectra (present Fig. 1 and van  
391 Haren et al., 2002) and in the continuum of the band  $[f N]$  in open-ocean T-spectra (van  
392 Haren and Gostiaux, 2009).

393 About 140 m above the seafloor, a less precise older-type T-sensor demonstrates  $p = -$   
394  $7/5$  between a reduced range of about  $10 < \omega < 1000$  cpd, with a suggestion for  $p = -5/3$   
395 around 10 cpd. This indicates convection can still dominate over shear extending  $O(100$  m)  
396 above the seafloor, as has been shown in more detail for certain periods (van Haren, 2023c).

397 Whilst more extended work with longer data sets and more T-sensors is to be done,  
398 the extended continuous spectral slope from these high-resolution temperature observations  
399 suggests a direct coupling between sub-mesoscale motions, IGW motions, comprising  
400 internal gravity and gyroscopic waves, and convection turbulence. The temperature spectra  
401 also show consistency with the limited KE-spectra of Fig. 1 from roughly the same area, and  
402 both indicate a dominance of non-isotropic, stratified-turbulence convection between sub-  
403 mesoscales and largest turbulent overturning scales in extended BO-scaling suggesting cross-  
404 spectral coupling. The discrepancy with KE-spectra in laboratory experiments of Pawar and  
405 Arakeri (2016) may be due to the difference of settings. In a non-zero-mean flow turbulence  
406 convection experiment near the gas-liquid critical point, BO-scaling was observed for both  
407 KE and temperature (Ashkenazi and Steinberg, 1999). We recall that our deep-sea conditions  
408 are non-zero-mean flow, weak tides, very high bulk Reynolds numbers  $O(10^5)$  given the large  
409 scales, varying non-zero vertical density stratification, and our example spectra did not clearly  
410 resolve KO-scaling.

411 This 18-day T-sensor data set demonstrates dominant deviations from inertial  
412 subrange over several orders of magnitude of frequency range. The mesoscale-IGW-  
413 turbulence motions transport and locally mix warm waters with cooler surroundings outside a  
414 period of buoyancy-driven dense-water formation, which is thought to bring cooler waters  
415 downward during short periods of time.

416

#### 417 **5 How robust is the system of ocean circulation and stratification?**

418 Any variation to the nonlinear system of ocean circulation may encounter several  
419 complex feedback mechanisms, of which the effects are not yet fully understood for the  
420 present-day ocean. Although stable density stratification hampers vertical exchange by

421 turbulent mixing, it does not block it. While stratification supports internal waves and their  
422 destabilizing shear, turbulent mixing during particular phase of a wave may decrease or  
423 destroy it locally in time and space. However, a subsequent internal wave-phase will restratify  
424 the mixed patch, thereby maintaining its own support of stable stratification. Such a feedback  
425 system may be at work, for example when the ocean absorbs more heat.

426         Increased sea-surface temperature may lead to increased vertical density  
427 stratification, which may lead to less turbulent exchange as vertical overturning is suppressed.  
428 However, it will also lead to more internal waves through the extension of their spectral band  
429 to higher frequencies, with the potential to increased interaction, non-linearity, and  
430 turbulence-generating wave breaking. As particular internal waves can propagate deep into  
431 the ocean interior away from their source, they can cause enhanced turbulent mixing  
432 elsewhere (e.g., Alford, 2003).

433         Limited observations have thus far not provided evidence for an inverse  
434 correspondence between changes in turbulent mixing and changes in temperature across the  
435 near-surface photic zone along a longitudinal section of the Northeast Atlantic Ocean (van  
436 Haren et al., 2021b). This lack of correspondence suggests a feedback mechanism at work  
437 mediating potential physical environment changes so that global warming may not affect  
438 vertical turbulent fluxes of heat, and thereby also of, e.g., carbon.

439         One such feedback mechanism may be convection-turbulence induced by internal  
440 waves and sub-mesoscale eddies. Renewed analysis of yearlong moored current meter data  
441 from the Irminger Sea, North-Atlantic Ocean, demonstrate a significant  $p = -11/5$  spectral  
442 slope at sub- and at super-inertial frequencies (Fig. 3). As was outlined in van Haren (2007),  
443 the area showed an IGW-band (1), for  $N = f$ , with dominant sub-inertial shear at small 8-m  
444 vertical scales despite the dominant internal tidal KE. The correspondence with the  
445 Mediterranean data of Fig. 1 is striking, including the one order of magnitude change in KE  
446 between sub- and super-IGW  $p = -11/5$ -slopes with similar  $p = -1$  bridge albeit uncertain  
447 crossing level, and similar heights of near-inertial peak despite the tidal peak in Fig. 3.



448           Moored deep-water observations (e.g., van Haren and Dijkstra, 2021; van Haren et  
449 al., 2024) have demonstrated BO-scaling at internal wave-turbulence frequencies smaller than  
450 the Ozmidov frequency, the largest scale at which isotropic 3D turbulent overturns can exist  
451 in a stratified environment. This bears similarity with ‘stratified turbulence’ having low  
452 Froude numbers at horizontal scales  $O(10-100)$  m exceeding the Ozmidov scale, and which  
453 includes nonlinear internal waves (Riley and Lindborg, 2008; Falder et al., 2016; Chini et al.,  
454 2022). Horizontal wavenumber  $k_h$ -spectra are presented arguing that a scaling of  $k_h^{-5/3}$  in fact  
455 reflects stratified turbulence outside the inertial subrange of isotropic 3D-turbulence.  
456 However, visual inspection also shows BO-scaling in several figures of Riley and Lindborg  
457 (2008). As the internal wave/turbulence range is associated with vertical Froude numbers  
458  $O(1)$ , stratified turbulence has been associated with ‘marginal stability’ in numerical  
459 modelling (Chini et al., 2022). Previously, marginal stability was described in the context of  
460 nonlinear flows (Abarbanel et al., 1984) and, e.g., explaining stratified North-Sea  
461 observations (van Haren et al., 1999).

462           While few ocean observations have been presented of BO-scaling thus far in  
463 comparison with KO-scaling, perhaps also because of the lack of precision of standard  
464 oceanographic instrumentation, coupling has not been established between convection and  
465 stratified small-scale turbulence with mesoscale motions. Likewise, complicating factors are  
466 spectral interruption by internal waves. However, internal wave trapping by mesoscale eddies  
467 has been well described (e.g., Kunze, 1985; Voet et al., 2024), and thus provides an obvious  
468 coupling between these motions. It is expected that such coupling may lead to strong  
469 nonlinearity of the internal waves that leads to turbulent mixing produced by wave breaking.  
470 Although such turbulent mixing is smaller than that induced by internal wave breaking above  
471 sloping topography, such coupling may be an important factor in downward transport of near-  
472 inertial energy that eventually breaks elsewhere, e.g., over topography.

473           As demonstrated using Mediterranean observations, not only convectively unstable  
474 cooler and/or saltier waters potentially lead to downward motions from the surface. Also, sub-  
475 mesoscale eddies and near-inertial waves can push stratified waters to the deep sea. Such a

476 downward push can be fast to transport materials from surface to 2500-m deep seafloor in a  
477 day (van Haren et al., 2006), and which is of the same order of magnitude as attributed to  
478 dense-water convection (Schott et al., 1996). It can also be more turbulent compared to shear-  
479 induced motions in the stratified ocean-interior, whereby turbulence reaches the seafloor  
480 according to few observations from the abyssal Pacific (van Haren, 2020) and alpine  
481 freshwater Lake Garda (van Haren and Dijkstra, 2021). Further extended observational  
482 evidence is urgently needed, preferably resolving much larger scales.

483         Although the anthropogenic influence on the Earth’s climate is without doubt, the  
484 impact on ocean circulation is not fully known because we lack sufficient, notably  
485 observational, information of the relevant processes that thus cannot be properly modeled yet.  
486 Therefore, we should be cautious in making predictions (e.g., Ditlevsen and Ditlevsen, 2023;  
487 van Westen et al., 2024) on future ocean circulation based on single parameters like ocean-  
488 surface temperature or fresh-water flux that are uncertain proxies. Because no observational  
489 (van Haren et al., 2021b), modeling (Little et al., 2020) or paleo-proxy validation (Cisneros et  
490 al., 2019) physics evidence exists that sea-surface temperature is a solid estimator of AMOC-  
491 strength variations, other properties like vertical density gradients (stratification), and  
492 turbulence intensity may be considered. Small-scale physical processes such as, for example,  
493 transport by sub-mesoscale eddies and turbulence-generating breaking of internal waves that  
494 are not incorporated in these models will alter such parameters, and thereby statistical  
495 analyses. This may lead to feedback mechanisms on property gradients such as density  
496 stratification so that large-scale ocean circulations like the AMOC may not collapse.

497         Variability of the ocean in space and time is a key to its dynamics, but it is unclear  
498 how robust such variations can be, e.g., whether shifting sites for deep dense-water formation  
499 (Gou et al., 2024) may be part of the same system. Observational evidence verifying  
500 numerical simulations’ outcome, not only predictions but also present-day, of ocean-state is  
501 needed. Observations are also required to demonstrate variability in relevant physics  
502 processes for model-implementation. Besides eddies and coupling with atmosphere (e.g.,  
503 Gent, 2018), numerical models of complex nonlinear ocean circulation should contain

504 internal-wave turbulence with appropriate space and time dependency. The importance of  
505 internal wave breaking leading to boundary mixing above sloping topography in general  
506 ocean circulation models has been acknowledged in various ways (Scott and Marotzke, 2002;  
507 Ferrari et al., 2016).

508         As for the ocean circulation in the horizontal plane near its surface with most impact  
509 on mankind, wind will remain the main driver. As long as the Earth rotation does not alter  
510 direction, wind will maintain its general course (Wunsch, 2004). The atmosphere remains the  
511 key player in the global heat transport across mid-latitudes rather than the ocean.  
512 Simultaneously, the importance of processes like stratification and turbulent mixing induced  
513 by, e.g., internal wave breaking with or without sub-mesoscale coupling cannot be  
514 underestimated for life near the ocean-surface as well as in the -deep, because it will come to  
515 a halt without such processes.

516

517 *Data availability.* No new data were created or analyzed in this study: replot and re-analysis  
518 of data presented in van Haren and Millot (2003), van Haren (2007) and van Haren (2023a).

519

520 *Competing interests.* The author declares that he has no conflict of interest.

521

522 *Acknowledgments.* I thank L. Gerringa for commenting on a previous draft of the manuscript.

523

524 **References**

- 525 Abarbanel, H. D. I., Holm, D. D., Marsden, J. E., and Ratiu, T.: Richardson number criterion  
526 for the nonlinear stability of three-dimensional stratified flow, *Phys. Rev. Lett.*, 52, 2352-  
527 2355, 1984.
- 528 Alb rola, C., Millot, C., and Font, J.: On the seasonal and mesoscale variabilities of the  
529 Northern Current during the PRIMO-0 experiment in the western Mediterranean Sea,  
530 *Oceanol. Acta*, 18, 163-192, 1995.
- 531 Aldama-Campino A., Fransner F.,  dalen, M., Groeskamp, S., Yool, A. D os, K., and  
532 Nycander, J.: Meridional ocean carbon transport, *Global Biogeochem. Cy.*, 34  
533 e2029GB006336, 2023.
- 534 Alford, M. H.: Redistribution of energy available for ocean mixing by long-range propagation  
535 of internal waves, *Nature*, 423, 159-162, 2003.
- 536 Ashkenazi, S., and Steinberg, V.: Spectra and statistics of velocity and temperature  
537 fluctuations in turbulent convection, *Phys. Rev. Lett.*, 83, 4760-4763, 1999.
- 538 Bak, P., Tang, C., and Wiesenfeld, K.: Self-organized criticality: An explanation of the  $1/f$   
539 noise, *Phys. Rev. Lett.*, 59, 381-384, 1987.
- 540 Bolgiano, R.: Turbulent spectra in a stably stratified atmosphere, *J. Geophys. Res.*, 64, 2226-  
541 2229, 1959.
- 542 Brainerd, K. E., and Gregg, M. C.: Surface mixed and mixing layer depths, *Deep-Sea Res. I*,  
543 42, 1521-1543, 1995.
- 544 Celani, A., Mazzino, A., and Vozella, L.: Rayleigh-Taylor turbulence in two dimensions,  
545 *Phys. Rev. Lett.*, 96, 134504, 2006.
- 546 Chini, G. P., Michel, G., Julien, K., Rocha, C. B., and Caulfield, C. P.: Exploiting self-  
547 organized criticality in strongly stratified turbulence, *J. Fluid Mech.*, 933, A22, 2022.
- 548 Chunchuzov, I. P., Johannessen, O. M., and Marmorino, G.O.: A possible generation  
549 mechanism for internal waves near the edge of a submesoscale eddy, *Tellus A*, 73, 1-11,  
550 2021.

551 Cisneros, M., Cacho, I., Frigola, J., Snchez-Vidal, A., Calafat, A., Pedrosa-Pàmies, R.,  
552 Rumín-Caparrós, A., and Canals, M.: Deep-water formation variability in the north-  
553 western Mediterranean Sea during the last 2500 yr: A proxy validation with present-day  
554 data, *Glob. Planet. Chang.* 177, 56-68, 2019.

555 Crepon, M., Wald, L., and Monget, J. M.: Low-frequency waves in the Ligurian Sea during  
556 December 1977, *J. Geophys. Res.*, 87, 595-600, 1982.

557 Ditlevsen, P., and Ditlevsen, S.: Warning of a forthcoming collapse of the Atlantic meridional  
558 overturning circulation, *Nat. Comm.* 14, 4254, 2023.

559 Emanuel, K., *Atmospheric Convection* 580 pp., Oxford Univ. Press, New York, 1984.

560 Eriksen, C. C.: Observations of internal wave reflection off sloping bottoms, *J. Geophys.*  
561 *Res.*, 87, 525-538, 1982.

562 Falder, M., White, N. J., and Caulfield, C. P.: Seismic imaging of rapid onset of stratified  
563 turbulence in the South Atlantic Ocean, *J. Phys. Oceanogr.*, 46, 1023-1044, 2016.

564 Ferrari, R., Mashayek, A., McDougall, T. J., Nikurashin, M. and Campin, J.-M.: Turning  
565 ocean mixing upside down, *J. Phys. Oceanogr.*, 46, 2229-2261, 2016.

566 Garrett, C.: The Mediterranean Sea as a climate test basin, In: Malanotte-Rizzoli, P., and  
567 Robinson, A. R. eds., *Ocean Processes in Climate Dynamics: Global and Mediterranean*  
568 *Examples*, Kluwer Academic Publishes, 227-237, 1994.

569 Garrett, C., and Munk, W.: Space-time scales of internal waves, *Geophys. Fluid Dyn.*, 3, 225-  
570 264, 1972.

571 Gascard, J.-C.: Vertical motions in a region of deep water formation, *Deep-Sea Res.*, 20,  
572 1011-1027, 1973.

573 Gascard, J.-C.: Mediterranean deep water formation, baroclinic eddies and ocean eddies,  
574 *Oceanol. Acta*, 1, 315-330, 1978.

575 Gent, P. R.: A commentary on the Atlantic meridional overturning circulation stability on  
576 climate models, *Ocean Mod.*, 122, 57-66, 2018.

577 Gerkema, T., Zimmerman, J. T. F., Maas, L. R. M., and van Haren, H.: Geophysical and  
578 astrophysical fluid dynamics beyond the traditional approximation, *Rev. Geophys.*, 46,  
579 RG2004, doi:10.1029/2006RG000220, 2008.

580 Gou, R., Wang, Y., Xiao, K., and Wu, L.: A plausible emergence of new convection sites in  
581 the Arctic Ocean in a warming climate, *Environ. Res. Lett.*, 19, 031001, 2024.

582 Gregg, M. C.: Scaling turbulent dissipation in the thermocline, *J. Geophys. Res.*, 94, 9686-  
583 9698, 1989.

584 Hosegood, P., Bonnin, J., and van Haren, H.: Solibore-induced sediment resuspension in the  
585 Faeroe-Shetland Channel, *Geophys. Res. Lett.*, 31, L09301, doi:10.1029/2004GL019544,  
586 2004.

587 Kolmogorov, A. N.: The local structure of turbulence in incompressible viscous fluid for very  
588 large Reynolds numbers, *Dokl. Akad. Nauk SSSR*, 30, 301-305, 1941.

589 Kunze, E.: Near-inertial wave propagation in geostrophic shear, *J. Phys. Oceanogr.*, 15, 544-  
590 565, 1985.

591 LeBlond, P. H., and Mysak, L. A.: *Waves in the ocean*, Elsevier, New York, 602 pp., 1978.

592 Lin, J.-T., *Turbulence spectra in the buoyancy subrange of thermally stratified shear flows*,  
593 143 pp., PhD-thesis Colorado State University, Fort Collins, 1969.

594 Liot, O., Seychelles, F., Zonta, F., Chibbaro, S., Coudarchet, T., Gasteuil, Y., Pinton, J.-F.,  
595 Salort, J., and Chillà, F.: Simultaneous temperature and velocity Lagrangian  
596 measurements in turbulent thermal convection, *J. Fluid Mech.*, 794, 655-675, 2016.

597 Little, C. M., Zhao, M., and Buckley, M. W.: Do surface temperature indices reflect  
598 centennial-timescale trends in Atlantic Meridional Overturning Circulation strength?  
599 *Geophys. Res. Lett.*, 47, e2020GL090888, 2020.

600 Liu, Z., Gu, S., Zou, S., Zhang, S., Yu, Y., and He, C.: Wind-steered eastern pathway of the  
601 Atlantic Meridional Overturning Circulation, *Nat. Geosci.*, 17, 353-360, 2024.

602 Lohse, D., and Xia, K.-Q.: Small-Scale properties of turbulent Rayleigh-Bénard convection,  
603 *Annu. Rev. Fluid Mech.*, 42, 335-364, 2010.

604 Marotzke, J., and Scott, J. R.: Convective mixing and the thermohaline circulation, *J. Phys.*  
605 *Oceanogr.*, 29, 2962-2970, 1999.

606 Marshall, J., and Schott, F.: Open-ocean convection: observations, theory, and models, *Rev.*  
607 *Geophys.*, 37, 1-64, 1999.

608 McDougall, T. J., and Ferrari, R.: Abyssal upwelling and downwelling driven by near-  
609 boundary mixing, *J. Phys. Oceanogr.*, 47, 261-283, 2017.

610 Mertens, C., and Schott, F.: Interannual variability of deep-water formation in the  
611 Northwestern Mediterranean, *J. Phys. Oceanogr.*, 28, 1410-1424, 1998.

612 Millot, C.: Circulation in the Western Mediterranean Sea, *J. Mar. Sys.*, 20, 423-442, 1999.

613 Munk, W.: Abyssal recipes, *Deep-Sea Res.*, 13, 707-730, 1966.

614 Munk, W., and Wunsch, C.: Abyssal recipes II: Energetics of tidal and wind mixing, *Deep-*  
615 *Sea Res. I*, 45, 1977-2010, 1998.

616 Obukhov, A. M.: Structure of the temperature field in a turbulent flow, *Izv. Akad. Nauk*  
617 *SSSR, Ser. Geogr. Geofiz.*, 13, 58-69, 1949.

618 Obukhov, A. M.: Effect of buoyancy forces on the structure of temperature field in a turbulent  
619 flow, *Dokl. Akad. Nauk SSSR*, 125, 1246-1248, 1959.

620 Pawar, S. S., and Arakeri, J. H.: Kinetic energy and scalar spectra in high Rayleigh number  
621 axially homogeneous buoyancy driven turbulence, *Phys. Fluids*, 28, 065103, 2016.

622 Perkins, H.: Observed effect of an eddy on inertial oscillations, *Deep-Sea Res.*, 23, 1037-  
623 1042, 1976.

624 Phillips, O. M.: On spectra measured in an undulating layered medium, *J. Phys. Oceanogr.*, 1,  
625 1-6, 1971.

626 Polzin, K. L., Toole, J. M., Ledwell, J. R., and Schmitt, R. W.: Spatial variability of turbulent  
627 mixing in the abyssal ocean, *Science*, 276, 93-96, 1997.

628 Polzin, K. L., Kunze, E., Toole, J. M., and Schmitt, R. W.: The partition of finescale energy  
629 into internal waves and subinertial motions, *J. Phys. Oceanogr.*, 33, 234-248, 2003.

630 Poujade, O.: Rayleigh-Taylor turbulence is nothing like Kolmogorov turbulence in the self-  
631 similar regime, *Phys. Rev. Lett.*, 97, 185002, 2006.

632 Reid, R. O.: A special case of Phillips' general theory of sampling statistics for a layered  
633 medium, *J. Phys. Oceanogr.*, 1, 61-62, 1971.

634 Rhein, M.: Deep water formation in the western Mediterranean, *J. Geophys. Res.*, 100, 6943-  
635 6959, 1995.

636 Riley, J. J., and Lindborg, E.: Stratified turbulence: A possible interpretation of some  
637 geophysical turbulence measurements, *J. Atmos. Sci.*, 65, 2416-2424, 2008.

638 Saint-Guilly, B.: On the response of the ocean to impulse, *Tellus* 24, 344-349, 1972.

639 Sarkar, S., and Scotti, A.: From topographic internal gravity waves to turbulence, *Ann. Rev.*  
640 *Fluid Mech.*, 49, 195-220, 2017.

641 Schott, F., Visbeck, M., Send, U, Fischer, J., and Desaubies, Y.: Observations of deep  
642 convection in the Gulf of Lions, Northern Mediterranean, during the winter of 1991/92, *J.*  
643 *Phys. Oceanogr.*, 26, 505-524, 1996.

644 Schuster, H. G., *Deterministic Chaos: An Introduction*, Physik-Verlag, Weinheim, 220 pp.,  
645 1984.

646 Scott, J. R., and Marotzke, J, 1998: The location of diapycnal mixing and the meridional  
647 overturning circulation, *J. Phys. Oceanogr.*, 32, 3578-3595, 2002.

648 Steffen, E. L., and D'Asaro, E. A.: Deep convection in the Labrador Sea as observed by  
649 Lagrangian floats, *J. Phys. Oceanogr.*, 32, 475-492, 2002.

650 Storer, B. A., Buzzicotti, M., Khatri, H., Griffies, S. M., and Aluie, H.: Global energy  
651 spectrum of the general oceanic circulation, *Nat. Comm.*, 13, 5314, 2022.

652 Taira, K., Yanagimoto D., and Kitagawa, S.: Deep CTD casts in the challenger deep. Mariana  
653 Trench, *J. Oceanogr.*, 61, 447-454, 2005.

654 Testor, P., and Gascard, J.C.: Post-convection spreading phase in the Northwestern  
655 Mediterranean Sea, *Deep-Sea Res.*, 53, 869-893, 2006.

656 Thorpe, S. A.: Transitional phenomena and the development of turbulence in stratified fluids:  
657 a review, *J. Geophys. Res.*, 92, 5231-5248, 1987.

658 Thorpe, S. A.: *The turbulent ocean*, Cambridge University Press, Cambridge, 439 pp, 2005.



659 van Haren, H.: Inertial and tidal shear variability above Reykjanes Ridge, *Deep-Sea. Res. I*,  
660 54, 856-870, 2007.

661 van Haren, H.: Slow persistent mixing in the abyss, *Ocean Dyn.*, 70, 339-352, 2020.

662 van Haren, H.: Convection and intermittency noise in water temperature near a deep  
663 Mediterranean seafloor, *Phys. Fluids*, 35, 026604, 2023a.

664 van Haren, H.: Near-inertial wave propagation between stratified and homogeneous layers, *J.*  
665 *Oceanogr.*, 79, 367-377, 2023b.

666 van Haren, H.: Direct observations of general geothermal convection in deep Mediterranean  
667 waters, *Ocean Dyn.*, 73, 807-825, 2023c.

668 van Haren, H., and Dijkstra, H. A.: Convection under internal waves in an alpine lake, *Env.*  
669 *Fluid Mech.*, 21, 305-316, 2021.

670 van Haren, H., and Gostiaux, L.: High-resolution open-ocean temperature spectra, *J.*  
671 *Geophys. Res.*, 114, C05005, doi:10.1029/2008JC004967, 2009.

672 van Haren, H., and Gostiaux, L.: Detailed internal wave mixing observed above a deep-ocean  
673 slope, *J. Mar. Res.*, 70, 173-197, 2012.

674 van Haren, H. and Millot, C.: Seasonality of internal gravity waves kinetic energy spectra in  
675 the Ligurian Basin, *Oceanol. Acta*, 26, 635-644, 2003.

676 van Haren, H., and Millot, C.: Rectilinear and circular inertial motions in the Western  
677 Mediterranean Sea, *Deep-Sea Res. I*, 51, 1441-1455, 2004.

678 van Haren, H., Maas, L., Zimmerman, J. T. F., Ridderinkhof, H., and Malschaert, H.: Strong  
679 inertial currents and marginal internal wave stability in the central North Sea, *Geophys.*  
680 *Res. Lett.*, 26, 2993-2996, 1999.

681 van Haren, H., Maas, L., and van Aken, H.: On the nature of internal wave spectra near a  
682 continental slope, *Geophys. Res. Lett.*, 29(12), 10.1029/2001GL014341, 2002.

683 van Haren, H., Millot, C., and Taupier-Letage, I.: Fast deep sinking in Mediterranean eddies,  
684 *Geophys. Res. Lett.*, 33, L04606, doi:10.1029/2005GL025367, 2006.

685 van Haren, H., Ribó, M., and Puig, P.: (Sub-)inertial wave boundary turbulence in the Gulf of  
686 Valencia. *J. Geophys. Res.Oceans*, 118, 2067-2073, doi:10.1002/jgrc.20168, 2013.

687 van Haren, H., Uchida, H., and Yanagimoto, D.: Further correcting pressure effects on  
688 SBE911 CTD-conductivity data from hadal depths, *J. Oceanogr.*, 77, 137-144, 2021a.

689 van Haren, H., Brussaard, C. P. D., Gerringa, L. J. A., van Manen, M. H., Middag, R., and  
690 Groenewegen, R.: Diapycnal mixing near the photic zone of the NE-Atlantic, *Ocean Sci.*,  
691 17, 301-318, 2021b.

692 van Haren, H., Voet, G., Alford, M. H., Fernandez-Castro, B., Naveira Garabato, A. C.,  
693 Wynne-Cattanach, B. L., Mercier, H., and Messias, M.-J.: Near-slope turbulence in a  
694 Rockall canyon, *Deep-Sea Res. I*, 206, 104277, 2024.

695 van Westen, R. M., Kliphuis, M., and Dijkstra, H.A.: Physics-based early warning signal  
696 shows that AMOC is on tipping course, *Sci. Adv.*, 10, eadk1189, 2024.

697 Voet, G., et al.: Near-inertial energy variability in a strong mesoscale eddy field in the Iceland  
698 Basin, *Oceanogr.*, 37, <https://doi.org/10.5670/oceanog.2024.302>, 2024.

699 Winters, K. B.: Tidally driven mixing and dissipation in the stratified boundary layer above  
700 steep submarine topography, *Geophys. Res. Lett.*, 42, 7123-7130, 2015.

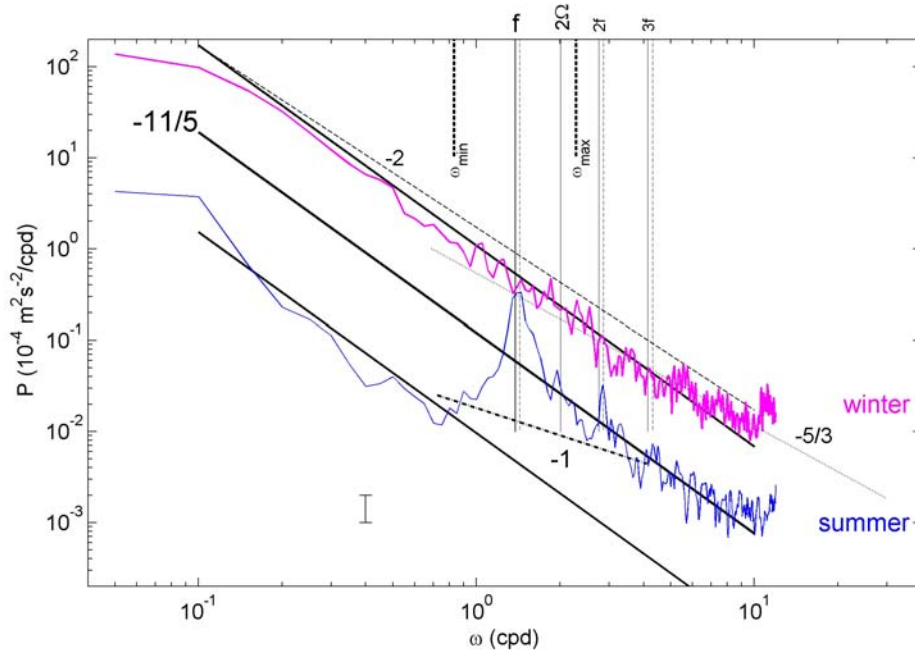
701 Wunsch, C.: Gulf Stream safe if wind blows and Earth turns, *Nature*, 428, 601, 2004.

702 Wunsch, C., and Ferrari, R.: Vertical mixing, energy and the general circulation of the oceans,  
703 *Ann. Rev. Fluid Mech.*, 36, 281-314, 2004.

704 Wynne-Cattanach, B. L., Couto, N., Drake, H. F., Ferrari, R., Le Boyer, A., Mercier, H.,  
705 Messias, M.-J., Ruan, X., Spingys, C. P., van Haren, H., Voet, G., Polzin, K., Naveira  
706 Garabato, A., and Alford, M. H.: Observational evidence of diapycnal upwelling within a  
707 sloping submarine canyon, *Nature*, 630, 884-890, 2024.

708 Xu, Y., and Fu, L.-L.: The effects of altimeter instrument noise on the estimation of the  
709 wavenumber spectrum of sea surface height, *J. Phys. Oceanogr.*, 42, 2229-2233, 2012.

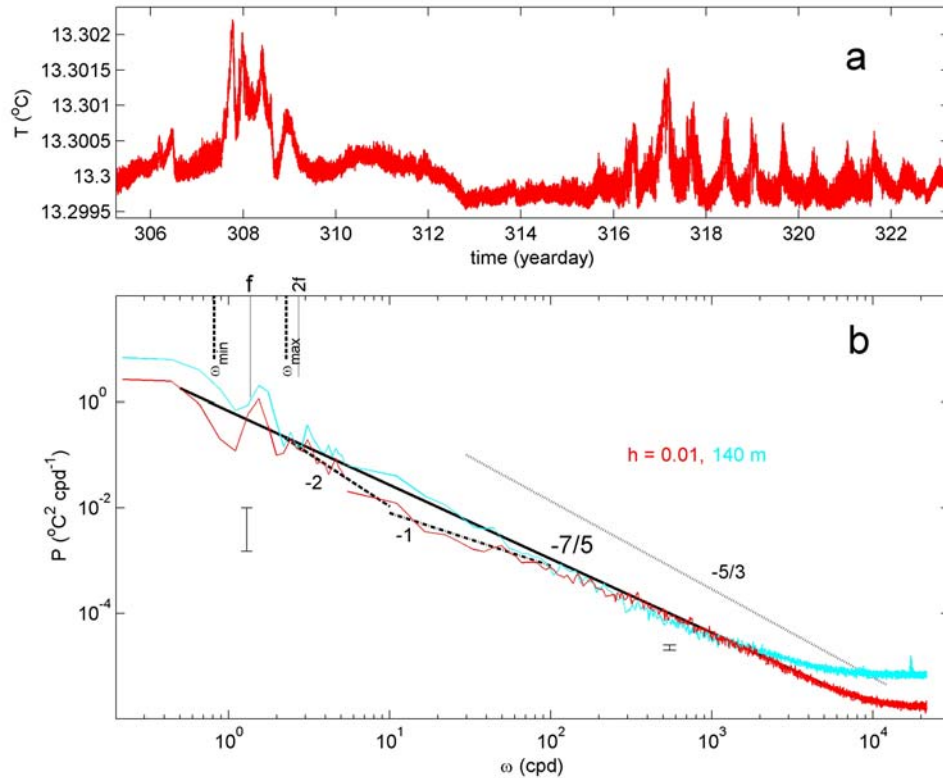
710



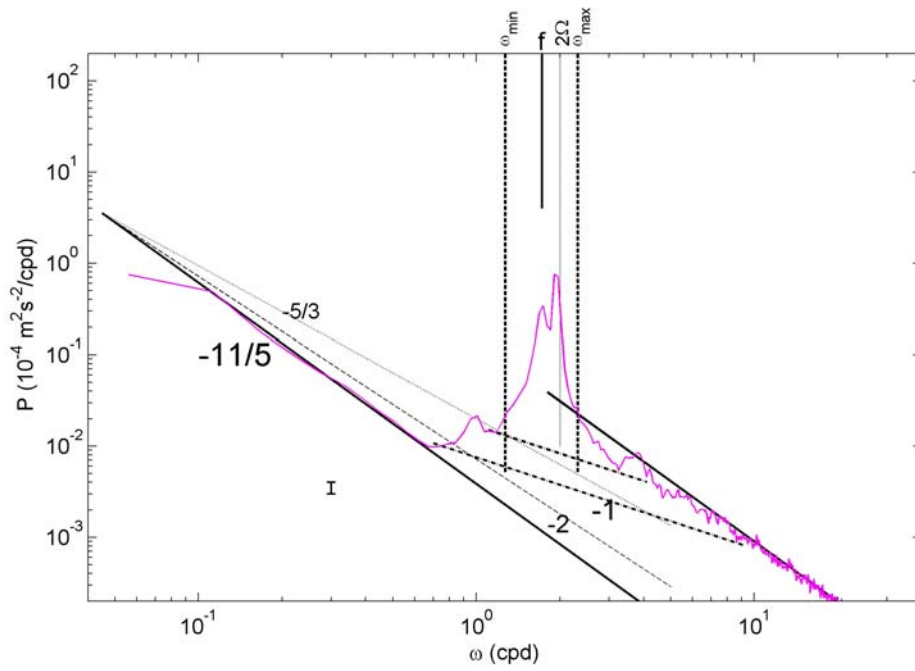
712

713 **Fig. 1.** Moderately smoothed (20 degrees of freedom, dof) kinetic energy (KE) spectra over  
 714 100 days of data from 3600-s sampled Aanderaa mechanical current meter moored in  
 715 1981/1982 at  $z = -1100$  m well above the continental slope in the Ligurian Sea at  $43^\circ 28.32'$   
 716 N,  $7^\circ 46.10'$  E, 2250 m water depth. For details on these data, see van Haren and Millot  
 717 (2003). The two spectra are not offset deliberately from each other; ‘noise’ also contains other  
 718 signals near the Nyquist frequency. The ‘summer’ spectrum (blue) is an average from data  
 719 between days 190 and 290 (in 1981), the ‘winter’ (magenta) between days 375 and 475  
 720 (adding +365 for days in 1982). Several frequencies are indicated including inertial frequency  
 721  $f$ , Earth rotational  $\Omega$  and inertio-gravity wave bounds [ $\omega_{\min} \leq f$ ,  $\omega_{\max} \geq N, 2\Omega$ ] for buoyancy  
 722 frequency  $N = f$ . The dashed lines indicate harmonics of  $1.04f$ . Four spectral slopes  $\omega^p$  are  
 723 indicated by their exponent:  $p = -11/5$  (solid slope in the log-log plot) for Bolgiano-Obukhov  
 724 ‘BO’ scaling reflecting the buoyancy subrange of convection-turbulence (e.g., Pawar and  
 725 Arakeri, 2016),  $p = -5/3$  (dotted slope) for Kolmogorov-Obukhov ‘KO’ scaling reflecting the  
 726 equilibrium inertial subrange for dominant shear-induced turbulence (Kolmogorov 1941;  
 727 Obukhov, 1949),  $p = -1$  (dash-dotted slope) for intermittency of self-organized criticality  
 728 (Schuster, 1984; Bak et al., 1987) and  $p = -2$  (dashed slope) for internal wave scaling (Garrett  
 729 and Munk, 1972) or finestructure contamination (Phillips, 1971; Reid, 1971).

730



731  
 732 **Fig. 2.** Eighteen days of high-resolution 2-s sampled temperature ‘T’ data from a NIOZ  
 733 T-sensor fallen off a mooring-line in 2020 and lying 0.01 m above a flat seafloor about 10  
 734 km south of the foot of the continental slope at 42° 49.50’ N, 6° 11.78’ E, 2458 m water  
 735 depth, about 100 km WSW from the site in Fig. 1. For details on these data see van Haren  
 736 (2023a). (a) Time series of 18 days of raw temperature data. (b) Temperature variance  
 737 spectrum that is stitched together using two spectra with different smoothing. Weakly  
 738 smoothed (10 dof;  $\omega < 5$  cpd) and heavily smoothed (250 dof;  $\omega > 5$  cpd) spectra of data in  
 739 a., with bars showing the respective 95% confidence limits. For comparison, a spectrum  
 740 is shown in cyan from data of a less precise T-sensor at a drag-parachute line stuck at 140  
 741 m above the seafloor. Frequency and spectral slope indications are as in Fig. 1, while -7/5  
 742 (solid slope) indicates BO-scaling of an active scalar (e.g., Pawar and Arakeri, 2016).  
 743 Note the different axes-ranges compared with Fig. 1.



744 **Fig. 3.** Like Fig. 1 with the same axes ranges, but for strongly smoothed (50 dof) KE  
 745 spectra averaged over 400 days of data from 600-s sampled Valeport mechanical current  
 746 meter moored at  $z = -1000$  m over the Mid-Atlantic Ridge at  $58^\circ 59.67' N$ ,  $33^\circ 56.12' W$ ,  
 747  $2540$  m water depth in 2003/2004, within the project discussed in van Haren (2007). The  
 748 small bar shows the 95% confidence interval.  
 749  
 750